AI-driven morphoclimatic regional frequency modelling of sub-daily rainfall-extremes

Andrea Magnini[1], Michele Lombardi[2], Taha B. M. J. Ouarda[3] and Attilio Castellarin[1]

1. Department of Civil, Chemical, Environmental and Materials Engineering (DICAM), University of Bologna, Bologna, Italy
2. Department of Computer Science and Engineering (DISI), University of Bologna, Bologna, Italy
3. Institut National de Recherche Scientifique (INRS), Quebec, Canada

Corresponding author: Andrea Magnini, andrea.magnini@unibo.it

Abstract

Common main limitations affect standard approaches to regional frequency analysis (RFA) of rainfall extremes. Our study focuses on three of them that are rather frequent: regional models address (a) a single duration, or (b) a single exceedance probability at a time, and/or (c) hold a small-to-medium homogeneous region only. We use unsupervised ensembles of artificial neural networks (ANNs) to set up four alternative RFA models of sub-daily rainfall extremes. These are fed with annual maximum series of rainfall depth of any length collected at 2238 raingauges in a large and climatically and morphologically heterogeneous region. Our models can predict parameters of a Gumbel distribution for any location within the study area and any duration in the 1-24 hours range. Prediction is based on mean annual precipitation (MAP), or on twenty morphoclimatic covariates. Validation is performed over an independent set of 100 gauges, where locally fitted Gumbel distributions are used as reference. A common literature approach where Gumbel parameters are functions of MAP is used as benchmark. Our results show that multivariate ANNs remarkably improve the estimation of percentiles relative to the benchmark approach. Finally, we show that the very nature of the proposed ANN models makes them suitable for interpolating predicted sub-daily rainfall quantiles across time-aggregation intervals

and space and can be adapted for considering more flexible target frequency distributions (e.g. 3-parameter models).

Keywords: neural networks, extreme rainfall, regional frequency analysis, Italy, sub-daily time-interval

1. Introduction

Several hydrological applications, such as the design and management of stormwater drainage systems, combined sewer overflows and flood control systems require an accurate estimation of the design storm (e.g., Claps et al., 2022; Camorani et al., 2005). The latter can be defined as the rainfall depth associated with a given duration and non-exceedance probability (commonly expressed in terms of return period). To produce an accurate estimation of the design storm, modelling the frequency regime of rainfall extremes in the location of interest is needed (e.g., Koutsoyiannis, 2007, Persiano et al. 2020). Timeseries of observed rainfall extremes (e.g., annual sequences of maximum rainfall depths for given durations), when locally available, are in many cases too short to perform robust at-site frequency analysis. This limitation is often addressed by means of regional frequency analysis (RFA), that consists in transferring observed data from other gauged locations to the target site (see e.g., Di Baldassarre et al. 2006, Castellarin et al. 2009, Blöschl, 2011).

In general, RFA consists of two main phases: (i) the delineation of a homogenous pooling-group of sites (i.e., region), containing gauged sites that are similar to the target one, and (ii) the definition of a regional model to transfer the information from the homogeneous region to the target site (e.g.,

Grimaldi et al., 2011). The scientific literature reports on a large number of different methods for conducting RFA of rainfall extremes (see e.g., Svensson and Jones, 2010). The homogeneous region is defined based on some hydrological similarity criteria (see e.g. Castellarin et al., 2001), and can be considered as fixed (i.e., the gauged sites are divided into fixed clusters) or specific for any target site, as in the region-of-influence approach (Burn et al., 1990). The regional transfer function defined in the second phase of RFA is highly variable depending on the specific approach: on the one hand, the target variable could be a specific percentile (e.g., Ouali et al., 2016), a parameter of a probability distribution (e.g., Soltani et al., 2017), a statistical moment or L-moment (e.g., Modarres and Sarhadi, 2011; Ngongondo et al., 2011), or the complete time series itself (e.g., Requena et al., 2017, 2018); on the other hand, the observations of the gauged sites could be used alone or with some covariates of the target variable. Literature also reports on several methods that do not require the definition of a homogeneous region (methods based on regression, e.g., Brath et al. 2003, or interpolation, e.g., Claps et al., 2022).

Regarding the application of RFA to the estimation of flood quantiles, the scientific community has proposed several approaches that make use of advanced artificial intelligence (AI) techniques. Linear and non-linear techniques have been discussed for the definition of a homogeneous region (e.g., Ouarda et al., 2001; Ouali et al, 2016). Models for regional flood frequency analysis can consider many morphological and climatic covariates (Msilini et al., 2022), consider non-linearity of the input-output relations (Ouarda and Shu, 2009), and represent the interaction between the input variables (e.g., Msilini et al., 2020). On the contrary, the literature does not report on many AI-aided RFA methods for modelling the frequency regime of extreme precipitation.

The preference for one model or another strongly depends on the specific case. Moreover, since certain knowledge of the frequency regime of a highly stochastic event is not possible, incontrovertible evaluation of regional models cannot be obtained (Di Baldassarre et al., 2009; Velazquez et al., 2011).

However, it is clear which are the characteristics that a good regionalization method should have. First, the ability to profitably use as much recorded information (i.e., observed data) as possible. This is due to the nature of available official gauging networks, that consist of unevenly distributed rain gauges, and timeseries that are often short or fragmented (Libertino et al., 2018; Kidd et al., 2017). As a result, very short sequences are often discarded in regional analysis (e.g., Di Baldassarre et al., 2006). Second, the model should be as flexible as possible. Due to the fast development of technology and science, the amount, location and type of data available is highly dynamic. Thus, a model that can be easily adapted to these changes has a great advantage.

In the present study, the potential of a new AI-based approach to RFA of rainfall extremes is investigated and discussed. It is based on ensembles of unsupervised artificial neural networks (ANNs), that are able to predict the parameters of a selected extreme value probability distribution of the dimensionless extreme rainfall for any duration between 1 and 24 hours. Following the general framework of the widely adopted storm index method (e.g., Di Baldassarre et al., 2006), the frequency regime of the dimensionless extreme rainfall is regionalized. This is the extreme rainfall depth timeseries divided by its mean value at each site for a given duration. In the present study we focused on the Gumbel distribution, but the approach could consider different models. The proposed method is simple, flexible, and innovative thanks to some characteristics. First, no clustering or target-pooling of available rain gauges is performed: all available annual sequences of maximum rainfall depth are used jointly. Second, no filter on a minimum length of annual sequences is needed and very short sequences (even with two observations) can be used. Third, training is performed simultaneously on all available durations, which leads to advanced interpolation of time-aggregation intervals capability, a very useful feature for practical applications such as the construction of intensity-duration-frequency curves (see Koutsoyiannis, 1998, Brath et al. 2003). Fourth, the modelled extreme value distribution can be

predicted at ungauged locations within the study region, based on available morphoclimatic information.

The proposed approach is tested in the present study by implementing it through four kinds of ANNs with increasing complexity. The first makes use of the mean annual precipitation (MAP) alone (MAP-ANN), which is a classical proxy for frequency regime of rainfall annual maxima (see e.g., Schaefer, 1990; Alila, 1999; Castellarin et al., 2009). The second relies on an extended set of twenty morphoclimatic characteristics of the site of interest, including MAP (EXT-ANN). The third (EXT-PCA-ANN) and the fourth (EXT-CCA-ANN) models are fed on pre-preprocessed versions of the same twenty input descriptors, that are obtained through principal component analysis (PCA), and canonical correlation analysis (CCA, see e.g., Di Prinzio et al., 2011).

We make use of a large dataset of gauged stations located in northern and central Italy. For each station, rainfall annual maximum series (AMS) for five different time-aggregation intervals, or durations for the sake of brevity, are available (i.e., 1h, 3h, 6h, 12h and 24h). The maximum length of the AMS series is 90 years. In particular, 2238 stations representing a wide range of morphological and climatic conditions are used to train the four models. Validation of the four regional models is performed using data collected at 100 independent raingauges. The validation considers a traditional RFA method based on L-moments and MAP (see e.g. Di Baldassarre et al., 2006) as the baseline regional approach (hereafter also referred to as MAP-Lm), as well as the newly proposed models (i.e., MAP-ANN, EXT-ANN, EXT-PCA-ANN, EXT-CCA-ANN), and compare their predictions with those resulting from at-site frequency analyses (i.e. locally estimated Gumbel distributions).

Finally, the study shows a preliminary application of the proposed EXT-ANN model that adopts the 3-parameter Generalized Extreme Value (GEV) distribution (Jenkinson, 1955). In this preliminary application, the parameter that controls the skewness of the GEV distribution (i.e., the shape

parameter) is regionalized through geostatistical interpolation procedure (e.g., Hengl, 2007), while the remaining two parameters are derived from the prediction of the EXT-ANN model. Testing the proposed approach for a 3-parameter distribution is important. The scientific literature clearly indicates that in some geographical and climatic contexts the flexibility of a 2-parameter Gumbel distribution, even though widely adopted in previous works (see e.g., Grieser et al., 2007; Svensson and Jones, 2010; Van den Besselaar et al., 2013; Piper et al., 2016; Maity, 2018; Caldas-Alvarez et al., 2022), is not enough for producing an accurate representation of the frequency of rainfall extremes (e.g., Koutsoyiannis and Baloutsos, 2000; Koutsoyiannis, 2004, Papalexiou et al., 2018).

Two main research questions are addressed within this research: (1) are ANNs useful and effective in RFA of rainfall extremes? (2) Are morphological indices helpful in describing the local frequency regime of sub-daily rainfall extremes?

2. Methods

The present Section describes the methodologies adopted to set up all the regional models considered in the study. It is divided into two parts: the first briefly summarizes the storm index model with the L-moments approach, that is considered as baseline; the second illustrates the theoretic principles of the ANN approach that originates the four AI-based models. More detail on the models' set-up is given in Section 4.

2.1 Storm index method and L-moments approach

The storm index method is one of the most commonly adopted models for RFA (Dalrymple, 1960; Brath et al., 2003). Given a certain target station where the rainfall depth needs to be estimated, and a group of gauged stations as homogenous region, the storm index method is described by equation 1.

$$h(d,T) = m_d \cdot h'(d,T) \qquad (1)$$

The rainfall depth associated with a given duration d and return period T , $h(d,T)$, is the product of a scale factor m_d, that is called the storm index, and the dimensionless rainfall depth $h'(d,T)$, that is called growth factor. The scale factor is site dependent and is usually estimated by averaging the available measurements at the target station or exploiting regional information through interpolation techniques. The growth factor is derived from a regional relation that is assumed to be valid for the entire homogenous group of sites, which requires to be defined.

Following the original version by Dalrymple (1960), several different applications of the storm index method have been proposed. The MAP-Lm model set up in the present study strictly follows the methods in Di Baldassarre et al. (2006), which in turn strongly relies on the findings of Schaefer (1990) and Alila (1999). These authors studied the extreme dimensionless rainfall depth, which is obtained by dividing the dimensional data by the mean depth associated with the same duration at the same station. They found that statistical moments and L-moments of extreme dimensionless rainfall are in relation to MAP. Thus, homogenous groups of stations can be identified according to their values of MAP, which can be used as a substitute of the geographical location and as proxy of extreme precipitation. Based on the findings by Hosking and Wallis (1997 and 1993), L-moments should be preferred for RFA to traditional moments as they are more robust to outliers, can characterize a wider range of distributions and are less subject to estimation bias.

In particular, the MAP-Lm model aims to estimate the regional growth factor of the dimensionless rainfall by means of a Gumbel distribution (i.e., generalized extreme value distribution with zero-value shape parameter; see cumulative density function $F(x)$, eq. 3) for each one of the considered durations (i.e., 1, 3, 6, 12, 24h). It is assumed that the whole study area can be described by the same regional laws between local MAP value and statistical moments of rainfall extremes; accordingly, the procedure

160 can be summarized in three major steps: (1) group gauged stations by their MAP values through a
161 moving window of 100 stations; (2) plot the average MAP and L-CV (i.e., L-coefficient of variation); (3) fit
162 the regional function L-CV(MAP) as solution of a least squares problem. This procedure is applied for
163 each duration to all stations with more than five years of measurement.

164 In detail, the relationship between L-CV and MAP is modelled by adopting a Horton-type curve (eq. 2).

165 $$L - CV = a + (b - a) \cdot \exp(-c \cdot MAP) \quad (2)$$

166 Once the *a*, *b* and *c* regional parameters are found, L-CV can be obtained in the target location as a
167 function of MAP with eq. 2. Then, using the relations described in Hosking and Wallis (1997), i.e., eq. 4
168 and 5, the location and scale parameters (α and ξ) of the desired local frequency distribution, which is a
169 Gumbel distribution in this case, are estimated.

170 $$F(x) = \exp\left(-\exp\left(-\frac{x-\xi}{\alpha}\right)\right) \quad (3)$$

171 $$\alpha = \lambda_2 / \ln(2) = (L - CV) \cdot \lambda_1 / \ln(2) \quad (4)$$

172 $$\xi = \lambda_1 - \gamma \cdot \alpha \quad (5)$$

173 Where λ_1, λ_2 and γ are in this order the L-moment of the first and second order (i.e., mean and the
174 standard deviation of the dimensionless AMS observed) and the Euler's constant (i.e., 1.504).

175 Despite relying on a single proxy for extreme rainfall, this model has been shown to be rather accurate
176 (Di Baldassarre et al., 2006) over the region for which it was proposed and tested. Moreover, the
177 general framework is rather flexible since local MAP values can be easily retrieved for various regions of
178 the world. For these reasons, it is selected as the baseline for evaluating the performance of the AI-
179 based approaches.

2.2 ANN approach

Artificial intelligence has been profitably used by several authors for enhancing RFA for floods (e.g., Msilini et al., 2020; Ouali et al., 2016b; Ouarda and Shu, 2009; Shu and Ouarda, 2007), and the accurate choice of models and manipulation of data shows encouraging results. However, the investigation of artificial intelligence techniques for rainfall RFA is not yet well documented.

In the present study, artificial intelligence is used to enhance efficiency in data exploitation and combination. We consider ensembles of unsupervised ANNs; four different models are set up: while fed with different input data, they are based on the same macro-structure. All the ANN models follow four general guidelines: (1) exploiting simultaneously the AMS with all the available durations; (2) using short timeseries as well as long ones; (3) minimizing negative logarithmic likelihood as objective function (see below); (4) predicting Gumbel distributions as target. Thus, differently from the MAP-Lm model, the timeseries from all the stations are pooled together for training and validating the ANN models. The aim of these ANNs, as for the MAP-Lm, is to estimate the growth factor of the storm index framework. This is done by finding the best parameters for Gumbel probability distributions of the dimensionless extreme rainfall for any duration at any location, that correspond to the minimum negative logarithmic likelihood. ANNs are among the most common machine learning models (Hastie et al., 2009). They consist of successive layers, each one containing a given number of neurons. Referring to each single *i-th* neuron, the output y_i is a function f_i of the linear combination of the n input factors $x_{i,j}$, as follows:

$$y_i = f_i\left(\sum_{j=1}^{n} w_{i,j} \cdot x_{i,j}\right) \quad (6)$$

Where w_j are the weights, or coefficients of the input factors, and f_i is assumed in the present study as a sigmoid function, as it is commonly done (e.g., Han and Moraga, 1995). The input factors for each neuron are the outputs from the previous layer, while for the first layer, the input are the descriptors themselves.

Before the training, the available dataset is divided into a "training/testing set" (the larger one), and a "validation set" (the smaller one, used only for the validation). During the training phase, the training/testing set is randomly divided into two subsets: a larger one that will be referred to as "training set", and a smaller one that is referred to as "testing set". Common proportions of data from the original training/testing dataset are 80% for the training and 20% for the testing set (e.g., see Xu et al., 2018). The best hyperparameter set (i.e., the weights $w_{i,j}$ for each *i-th* neuron) is searched while observing the training set) and minimizing the negative logarithmic likelihood function (logLH, see eq. 7) computed on the remaining data included in the testing set.

$$\log L\,H \;=\; \log\left(\prod_{k=1}^{m} p(x_k)\right) = \sum_{k=1}^{m} \log\big(p(x_k)\big) \qquad (7)$$

where m is the testing set.

Since ANNs are complex and accurate models, they are likely to learn how to perfectly reproduce the training set while being inaccurate with other datasets. This is referred to as overfitting. To improve the generalization ability and stability of a single ANN, an ANN ensemble can be used. It consists of a number of ANNs whose individual results are combined to generate a unique output. Many approaches have been proposed for generating single ANNs for the ensemble models (Breiman, 1996a) and integrating the multiple outputs (Breiman, 1996b). In the present study, ANNs are generated through bagging, and averaging is used for merging the results. Thus, for each single ANN, the same initial training/testing set is randomly split, as discussed above, so that the optimal hyperparameter set is searched by training the model on the training set while optimizing the objective function for the testing set. This method is a simple and effective way to obtain ANN ensemble models (see e.g., Shu and Burn, 2004; Shu and Ouarda, 2007).

3. Study region and morphoclimatic descriptors

3.1 Study region

The methods explained above are applied on a dataset of 2338 gauged locations. These are located in a wide geographical area in northern and central Italy (Figure 1), where a variety of climatic and morphological systems can be found. The north is dominated by the Alps, the highest Italian mountain chain, with a mean elevation of 2500 m.a.s.l., and highest peaks until 4800 m.a.s.l. The largest Italian plain, the Po plain, stretches in the southern border of the Alps, following the course of the Po river from the northwest to the northeast, where low coasts are located. The southern border of the Po plain is marked by the Northern Apennines, whose maximum peak is 2165 m.a.s.l. Within the study area, one of the factors that seem to have the largest effect on the precipitation regime is altitude (Allamano et al., 2009; Marra et al., 2021; Mazzoglio et al., 2022).

Three different datasets (Table 1) are used in the present study to derive the input information and set up the models described in Section 2. First, the Annual Maxima Series (AMS), the variable whose probability distribution needs to be estimated, are retrieved from the dataset I^2-RED (Mazzoglio et al., 2020). It includes annual maximum rainfall depths for 1, 3, 6, 12 and 24 consecutive hours from 2338 weather stations across the study area, recorded between 1916 and 2019. While 2238 stations have been selected and used as training/testing set for the five models (i.e. 80% for training and 20% for testing, see Section 2.2), the remaining 100 are used as a validation set (see Figure 1). The selection of the validation set is based on three main guidelines: (1) to identify a significant number of timeseries, so to have an informative validation set for evaluating the RFA models' performance; (2) to have gauges that are representative of the entire dataset in terms of location, local climate and morphological conditions (see Figure 1.c and 1.d); (3) to have long timeseries for using as reference validation values

247 the at-site predictions of rainfall quantiles (Figure 1.b). Training/testing and validation sets include
248 timeseries with at least 50 years of measurement (i.e., 248 for the training/testing set and 29 for the
249 validation set, see Figure 1.b).

250 The second dataset used in our study is the multi-error removed improved terrain model (MERIT, see
251 Yamazaki et al., 2017) DEM (see Figure 1), that was used to derive the morphological descriptors (lines 1
252 to 14 of Table 1).

253 A third dataset was used in the analysis for retrieving the climatic information, that is the ISPRA
254 BIGBANG dataset (i.e., version 4.0, see Braca et al., 2018), that contains, among other variables, a 1km
255 raster representation of the annual totals of cumulative liquid and snow precipitation over the 1951-
256 2019 time interval.

257

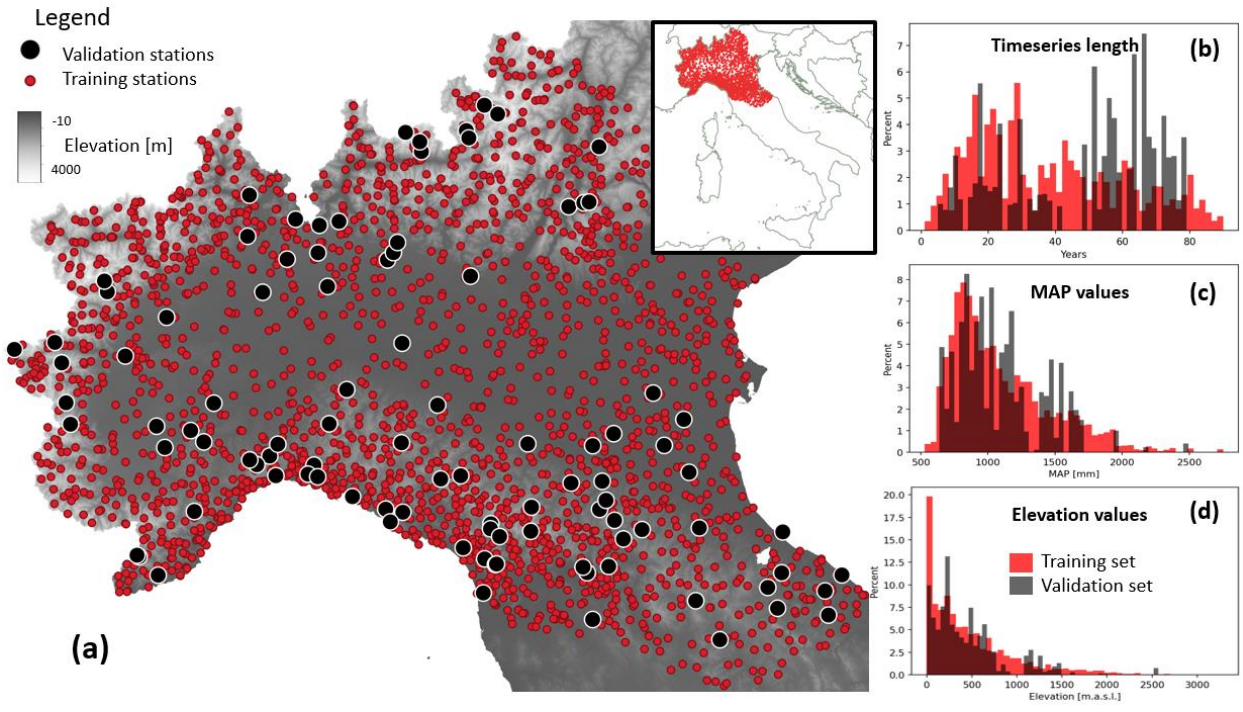

258

Figure 1: *Study area, training/testing (red dots) and validation (black dots) raingauges (panel a); sample frequency distribution (%) of several characteristics for the training/testing (red bars) and validation (grey bars) raingauges: timeseries length (panel b), mean annual precipitation (or MAP, panel c), and elevation (panel d).*

3.2 Morphoclimatic descriptors

The descriptors adopted in the present study were selected based on Mazzoglio et al. (2022), which explored the influence of climatic and morphological descriptors on the statistics of rainfall extremes. They can be divided into three groups: morphological, climatic and geographical. The first group includes descriptors of the elevation, slope and aspect within a distance of 1km from the station of interest (i.e., from 1 to 6 of Table 1), and of the orography and distance between the station and the sea coastlines (i.e., from 7 to 14 of Table 1). The climatic descriptors include mean annual rainfall and snow, and their multi-year standard deviation (i.e., from 15 to 18 of Table 1). The geographic descriptors consist of longitude and latitude (i.e., 19 and 20 of Table 1).

Descriptor	Description	Information origin
1	mean altitude within a distance of 1km from the gauged location	MERIT DEM
2	standard deviation of the altitude within a distance of 1km from the gauged location	MERIT DEM
3	mean slope (I.e., ration between vertical and horizontal distance) within a distance of 1km from the gauged location	MERIT DEM

4	standard deviation of the slope within a distance of 1km from the gauged location	MERIT DEM
5	mean aspect (I.e., direction of maximum slope) within a distance of 1km from the gauged location	MERIT DEM
6	the standard deviation of the aspect within a distance of 1km from the gauged location	MERIT DEM
7	minimum distance from the Adriatic coast	MERIT DEM
8	mean elevation within the distance between the gauged location and the Adriatic coast	MERIT DEM
9	standard deviation of elevation within the distance line between the gauged location and the Adriatic coast	MERIT DEM
10	Maximum elevation within the distance line between the gauged location and the Adriatic coast	MERIT DEM
11	minimum distance from the Tyrrhenian coast	MERIT DEM
12	mean elevation within the distance between the gauged location and the Tyrrhenian coast	MERIT DEM
13	standard deviation of elevation within the distance line between the gauged location and the Tyrrhenian coast	MERIT DEM
14	Maximum elevation within the distance line between the gauged location and the Tyrrhenian coast	MERIT DEM
15	Mean annual precipitation	BIGBANG dataset
16	Mean annual snow precipitation	BIGBANG dataset

17	Standard deviation of annual precipitation within the 1919-2019 record period	BIGBANG dataset
18	Standard deviation of annual snow precipitation within the 1919-2019 record period	BIGBANG dataset
19	Longitude	I^2-RED
20	Latitude	I^2-RED

Table 1: *Input descriptors and source dataset used for retrieving them (references for MERIT DEM, BIGBANG and I2-RED datasets are Yamazaki et al., 2017, Braca et al., 2018, Mazzoglio et al., 2020, in this order.*

The study descriptors can be obtained through GIS processing procedures of freely available datasets: a digital elevation model (DEM) is needed for retrieving the morphological descriptors, a precipitation dataset for the climatic group, and the coordinate of the gauged stations themselves for the geographical descriptors.

Some descriptors show significant inter-correlation, as illustrated by the correlation matrix depicted in Figure 2. Each element X_{ij} of this square and symmetric matrix is the Pearson's correlation coefficient

(PCC) of descriptors X_i and X_j. The PCC varies between –1 and 1, and the higher its absolute value is, the higher is the correlation between the two variables to whom it is referred.

$$PCC(X_i, X_j) = \frac{cov(X_i, X_j)}{var(X_i) \cdot var(X_j)} \quad (8)$$

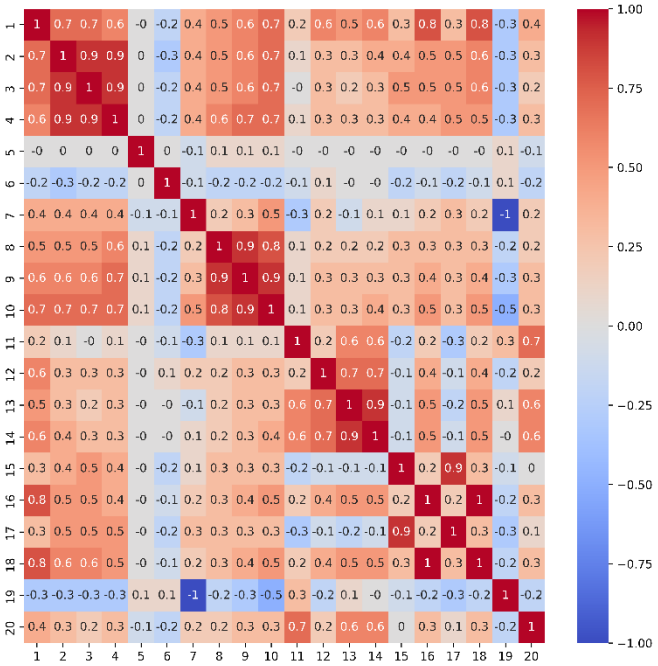

Figure 2: *Correlation matrix (i.e., matrix whose elements are PCC) of input descriptors, reported in the same order as in table 1*

Several groups of highly inter-correlated variables are evident (e.g., 1-4, see Figure 2), and the mean altitude (descriptor 1) is strongly correlated with most of the other descriptors. This characteristic of the dataset is common, and several authors, as Di Prinzio et al. (2011), showed that pre-processing input datasets by means of Principal Component Analysis (PCA, Jolliffe, 2002) or Canonical Correlation Analysis (CCA, Hotelling 1935), and removing redundant information may improve the training efficiency of data-driven methods and may result in better predictions. To test the convenience of preprocessing

techniques for the present study case, PCA and CCA are adopted for two out of the four ANN models trained (see Section 4).

Finally, climate indexes used in our study (i.e., descriptors 15, 16, 17 and 18) are long-term averages referring to a given climate time-window (i.e. 1951-2019). Hence, we do not consider possible non-stationarities in our study, which is an interesting subject for future developments (see e.g. Persiano et. al., 2020 for indications of signals on non-stationarity in sub-daily rainfall extremes for the study region).

3.3 Gumbel target frequency distribution

Figure 3 illustrates the L-moments ratio diagram (see e.g. Hosking and Wallis, 1997) of the study the rainfall annual maximum series at 1h and 24h durations. Regardless of the duration, a high variability of sample L-moments is evident, as it was expected; the location of the weighted average is a point on the GEV line, very near to the point indicating the theoretical L-moments of the Gumbel distribution.

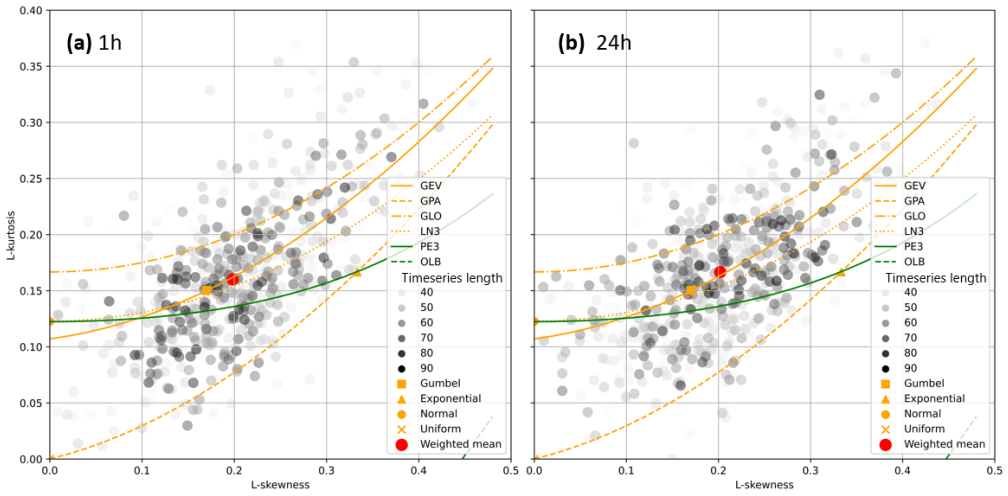

Figure 3: *L-moments ratio diagram of the 2338 gauged stations (i.e., training/testing and validation set) for annual maximum series with 1h (a) and 24h (b) duration.*

Thus, the choice of a regional distribution type is restricted to be either a Gumbel or a GEV. Several studies (e.g., Koutsoyiannis et al. 2000, 2004; Papalexiou and Koutsoyiannis, 2013) showed how the

309 latter should be preferred for a better estimation of the upper tail in some geographical and climatic
310 contexts. However, these studies also made it clear that the estimation of the shape parameter of a GEV
311 distribution is affected by high uncertainty, especially when short time series are used. Due to this
312 reason, several recent studies proposing RFA approaches still resort to the more robust Gumbel
313 distribution (e.g., Svensson and Jones, 2010; Maity, 2018; Ouarda et al., 2019; Caldas-Alvarez, 2022).
314 Thus, our study thoroughly assesses the viability of the Gumbel target distribution for the proposed ANN
315 RFA models. Nevertheless, for the sake of generalization, we also briefly present a possible adaptation
316 of the proposed approach to the GEV distribution.

317

318 # 4. Regional ANN models

319 ## 4.1 ANN models with Gumbel target frequency distribution

320 We set up and analyze four different regional ANN models, all consisting of ensembles of ANNs. As the
321 MAP-Lm model (see Sect. 2.1), they all aim to produce a regional estimate of the local growth factor for
322 the dimensionless extreme rainfall depth associated with in a given duration (or time aggregation
323 interval). Therefore, they are trained on dimensionless AMS of rainfall depths for a set duration, that are
324 obtained by dividing the original annual sequence by its sample mean (see details later on).

325 The first model is referred to as MAP-ANN and is fed exclusively on the MAP descriptor. Its application
326 and validation allow it to investigate the effect of exploiting the same input information as in the MAP–
327 Lm method (i.e., MAP) with a different model (i.e., ANN) that exploits all available timeseries of the
328 training set and is simultaneously trained with all available durations (i.e., 1h, 3h, 6h, 12h and 24h). The
329 second model, EXT-ANN, is fed on the extended dataset composed of all the descriptors considered (see
330 Table 1). It is an example of both a multivariate approach to RFA of rainfall extremes and a machine

learning-based way to exploit multiple input information. The third and fourth models (EXT-PCA-ANN and EXT-CCA-ANN, respectively) make use of preprocessed versions of the same input descriptors of EXT-ANN through PCA and CCA, respectively.

PCA is a statistical technique for reducing the dimensionality of a dataset (Jolliffe, 2002, Di Prinzio et al., 2011). This is accomplished by linearly transforming the data into a new coordinate system where most of the variation in the data can be described with fewer dimensions than the initial dataset. This consists of a change of basis of the original data matrix, and the new dimensions are the principal components (or PCs). Given a set of *r* variables ($X = (X_1, X_2, \dots, X_r)$), the covariance matrix is computed, where each element a_{ij} is the covariance between the *i-th* and *j-th* variables. The PCs are eigenvectors of the covariance matrix of the original data. The higher the number of selected PCs, the higher amount of variance of the initial matrix is caught. In this study, the variance chosen for reducing the dimensionality of the descriptors' space is 80%, that corresponds to five PCs: these are the input covariates for the EXT-PCA-ANN model. We select this threshold to allow the model to represent most of the variability of the system, yet eliminating the noise affecting the signal.

CCA (Hotelling 1935, Di Prinzio et al., 2011) is a multivariate analysis technique used to identify the possible correlations between two groups of variables. It consists of a linear transformation of two groups of random variables into pairs of canonical variables, which are established in such a way that the correlations between each pair are maximized. With specific reference to our case, the set of right-hand random variables X consists of the *r* input descriptors ($X = (X_1, X_2, \dots, X_r)$, where *r* equals twenty). As the left-hand set of variables, the *s* L-coefficients of variation of the AMS for each station for the analyzed durations are selected ($Y = (L\text{-}CV_{1h}, L\text{-}CV_{3h}, L\text{-}CV_{6h}, L\text{-}CV_{12h}, L\text{-}CV_{24h})$, where *s* is five). The objective of CCA is to construct linear combinations V_i and W_i (called canonical variables) of the variables X and Y, as follows:

$$V_i = A_{i1} \cdot X_1 + A_{i2} \cdot X_2 + \cdots + A_{i20} \cdot X_{20} \quad (9)$$

$$W_i = B_{i1} \cdot L - CV_{1h} + B_{i2} \cdot L - CV_{3h} + \cdots + B_{i5} \cdot L - CV_{24h} \quad (10)$$

where *i = 1, ... , p*, with *p = min (r, s)*. The first weights vectors A_1 and B_1 maximize the correlation coefficients between resulting canonical variables, under constraints of unit variance. Once the first pair of canonical variables is identified, other pairs can be obtained under the constraint that the correlation between V_i and W_i is 0 (where i ≠ j). The five canonical variables derived from the canonical transformation of the twenty input descriptors are used as input covariates of the EXT-CCA-ANN model.

The EXT-PCA-ANN and EXT-CCA-ANN models provide the opportunity to assess the effect of PCA and CCA pre-processing techniques. It will be discussed whether the preprocessed input descriptors are able to effectively reproduce the variability of the problem, while the noise in the real signal is absent.

The workflow for setting-up and validating the ensemble ANN models is summarized in Figure 4. For a stable training of the ANNs, the input to the four regional ANN models, which include the dimensionless AMS and the considered morphoclimatic descriptors, is standardized (see e.g., Milligan et al., 1988, Jain et al., 2005). Each standardized input ($X_{i,\,st}$) is obtained from the original input (X_i) by subtracting the regional mean (μ_i, mean of X_i over the whole training/testing set) and by dividing this difference by the regional standard deviation (σ_i, standard deviation of X_i over the whole training/testing set).

$$X_{i,\,st} = \frac{X_i - \mu_i}{\sigma_i} \quad (11)$$

The same relations used for standardizing the training/testing set (with the same μ_i and σ_i, see T1 in Fig. 3), are used also for the validation set (process V1 in Fig. 3). Accordingly, the ensemble ANN models predict Gumbel parameters for standardized and dimensionless distributions at the 100 validation sites, and these parameters need to be back-transformed to the dimensionless space (see process V3, Fig. 3). This is done through two empirical linear relations (i.e., one for the location parameter and one for the

scale parameter) between the parameters of the locally fitted Gumbel distribution that model the frequency of the dimensionless AMS and the standardized AMS (see S1, S2 and S3 of Fig. 3).

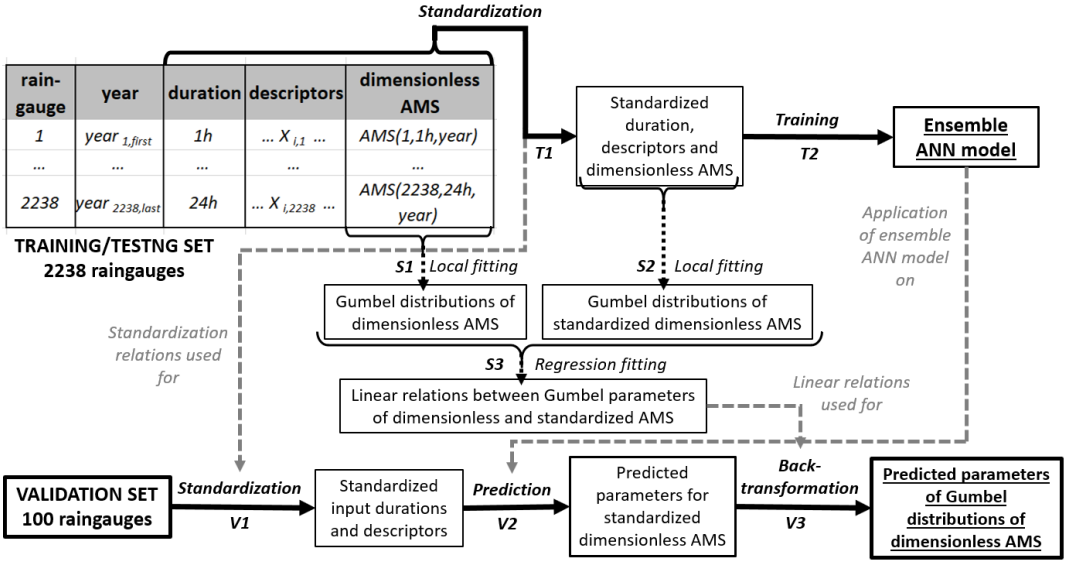

Figure 4: *Workflow for setting-up and validating the ANN models. Main processes for training (T1 and T2) and validation (V1, V2 and V3) are marked with solid black arrows; side processes (i.e., S1, S2 and S3) marked with dotted black arrows. Models and relations defined in the training phase and used for validation are marked with dashed grey arrows.*

After some preliminary experiments with different structures of the models, ensembles of 15 ANNs, each one with four layers, were found to be a good balance between prediction accuracy and computational resources required for training.We tested different proportions for splitting the training/testing set into the training and testing set (e.g., 70%-30% and 80%-20%), but we did not observe significant variations in the results. Thus, we opted for the 80%-20% configuration, since it used a larger amount of data for the training set.

4.2 ANN models with GEV target frequency distribution: a preliminary assessment

The approach we propose is general, and can be adapted to any distribution. In particular, the usage of more flexible, 3-parameter probability distributions may allow a better representation of the highest rainfall percentiles. Nevertheless, the estimation of three parameters might be highly uncertain, even when state-o-the-art fitting methods are adopted for at-site frequency analysis (see Section 3.3). Hence, in case the proposed ANN approach makes use of a 3-parameter distribution (or even a 4-parameter one), the usage of very short timeseries should be carefully considered both for training the models and for validating them. The findings of these test experiments may be different from case to case. Thus, in this Section we show a preliminary adaptation of the ANN models with the GEV distribution, that has to be intended as a demonstration of the flexibility of the proposed approach.

The GEV distribution is characterized by three parameters. The third parameter (i.e., the shape) controls the upper tail of the distribution, and is directly linked to the skewness of the distribution, e.g. expressed in terms of L-CS (see Hosking and Wallis, 1997). The remaining two parameters, location and scale, depend on the third one, but are also linked to the first and second L-moments, similarly to the Gumbel case. The GEV distribution and the mathematical relationships between its parameters and the L-moments can be found in Hosking and Wallis (1997) and are not reported here for the sake of brevity.

We adapted our EXT-ANN model to the GEV distribution and validated it for the same 100 validation sites by following four steps:

1. The sample L-coefficient of skewness (L-CS) is computed for the timeseries within the training/test set having at least 30 years of data
2. The sample L-CS values from step 1 are regionalized across the study area by a geostatistical interpolation technique (Hengl, 2007)
3. For any given raingauge belonging to the 100-sites validation set,
    a. the shape parameter of the GEV is estimated based on the regionalized L-CS value

b. the local LCV value is obtained from the Gumbel scale parameter predicted by EXT-ANN with eq. 4

c. the L-CV value from step 4 and shape parameter from step 3 are used for deriving the remaining parameters of the GEV distribution

4. The resulting ANN model is compared with a GEV distribution whose shape parameter results from pervious step 3.a, while location and scale parameters are fitted using an at-site maximum likelihood procedure

Step 2 adopts the ordinary kriging (OK) method as preliminary analyses using more complex approaches (i.e., kriging with external drift, universal kriging, see Hengl, 2007) did not improve our results. Details on the OK method can be found in several studies (e.g., Shehu, 2023; Hengl, 2007).

This application of the EXT-ANN model will be hereinafter referred to as EXT-ANN-GEV.

5. Performance metrics used in validation

The evaluation of the five models (i.e., baseline, MAP-ANN, EXT-ANN, EXT-PCA-ANN, EXT-CCA-ANN) is conducted by considering three aspects of the models' output Gumbel distributions: the scale parameters, and the 80^{th} and 99^{th} percentiles. The true values are the ones related to the Gumbel probability distributions fitted on the validation dataset with the maximum likelihood method.

Three metrics are computed to evaluate the models' performance from a global point of view: relative BIAS (BIASr), root mean squared error (RMSE), and Pearson's correlation coefficient (PCC, see Section 3). The first two are commonly used in literature (e.g., see Msilini et al., 2020; Ghamariadyan and Imteaz, 2021; Shu and Ouarda, 2007), and quantify the systematic error of the models (BIASr) and the gap between the predicted and expected values of the considered variables (RMSE). Differently, the PCC

does not take into account the actual values of the variables, since it simply measures the degree of linearity of the relationship between the empirical reference values and the corresponding model's predictions.

$$BIASr = \frac{1}{n}\sum_{i=1}^{n}\left(\frac{y_i - y_{i,pred}}{y_i}\right); \quad n = \sum_{j=1}^{n_t} n_j \qquad (18)$$

$$RMSE = \sqrt{\frac{1}{n}\sum_{i=1}^{n}\left(y_i - y_{i,pred}\right)^2} \qquad (19)$$

Where *n* is the total number of validation observations (i.e., for a given duration, the sum of the total years of annual maxima records n_j over the n_t validation stations), and each annual maximum is considered as a single *i-th* observation. Thus, any station is counted as many times as its timeseries length (see also Figure 4), and the final metrics mainly depend on the longest timeseries. While y_i is the true value of the output variable (i.e., the one related to the fitted Gumbel distributions) for the *i-th* observation, $y_{i,pred}$ is the value of the output variable obtained with the regional model.

One more metric is computed to evaluate models' accuracy for each single station and each single duration. This is herein referred to as percent relative error (PRE) and defined as in eq. 14.

$$PRE\,[\%] = \frac{y_{pred} - y}{y} \cdot 100 \qquad (20)$$

Positive values of PRE represent overestimation with respect to the true values (*y*), while negative ones account for underestimation.

6. Validation of the Regional Models

After training, the five models described in Sections 2 and 4 (i.e., MAP-Lm, MAP-ANN, EXT-ANN, EXT-PCA-ANN and EXT-CCA-ANN) are used to predict Gumbel distributions for the dimensionless annual

maximum rainfall at the locations of the validation stations. We considered the performance metrics associated with the estimation of the Gumbel scale parameters and two dimensionless rainfall quantiles, namely the quantiles associated with the 0.8 and 0.99 non-exceedance probabilities.

	scale				
metrics	**MAP-Lm**	**MAP-ANN**	**EXT-ANN**	**EXT-PCA-ANN**	**EXT-CCA-ANN**
			1h		
BIASr	*-0.075*	-0.038	-0.051	**-0.025**	-0.046
RMSE	*0.050*	0.049	*0.050*	**0.048**	**0.048**
PCC	0.120	*0.105*	0.242	0.252	**0.275**
			3h		
BIASr	*-0.083*	-0.046	-0.053	**-0.044**	-0.047
RMSE	*0.050*	0.047	**0.044**	**0.044**	**0.044**
PCC	-0.031	*0.015*	**0.422**	0.387	0.394
			6h		
BIASr	*-0.081*	-0.048	-0.047	-0.060	**-0.038**
RMSE	*0.050*	0.048	**0.043**	0.045	0.044
PCC	*-0.037*	0.176	**0.453**	0.387	0.384
			12h		
BIASr	*-0.068*	-0.046	**-0.029**	-0.051	-0.030
RMSE	*0.049*	0.048	**0.042**	0.045	0.045
PCC	*-0.063*	0.204	**0.463**	0.337	0.350
			24h		
BIASr	*-0.079*	-0.061	**-0.045**	-0.050	**-0.045**
RMSE	*0.048*	0.047	**0.039**	0.042	0.042
PCC	*0.030*	0.139	**0.548**	0.421	0.420

Table 2: *Performance metrics for estimated scale parameter for Gumbel distributions of dimensionless annual maxima at 100 validation points. For each duration, the best case for each metric is marked in bold, while the worst is in italic.*

Concerning the metrics for the scale parameters (see Table 2), it is possible to observe that RMSE and PCC present a similar behavior across durations and models, which differs from the outcomes in terms of BIASr. Indeed, RMSE and PCC tend to show optimal values for the same regional model, which is often different from the regional model characterized by the smallest BIASr. The value of BIASr is generally between a few % and 9% for the scale parameters. Overall, the estimation of a regional model for the 1h duration seems to be more complex than for higher durations, as it is pointed out by higher values of the PCC for 12 and 24h. The MAP-Lm model is the least accurate according to the RMSE and PCC metrics, while the MAP-ANN model is the second-to-least accurate, but it is still slightly better than the MAP-Lm. Even though the EXT-ANN, EXT-PCA-ANN and EXT-CCA-ANN models have similar performances, the preprocessing of data leads to a better performance of EXT-PCA-ANN and EXT-CCA-ANN compared to the EXT-ANN model for the 1h duration, while the EXT-ANN is the best one for durations of 6, 12 and 24h.

The metrics computed for the 80th and 99th percentiles are reported in Table 3.

80th percentile							**99th percentile**						
metrics	**MAP-Lm**	**MAP-ANN**	**EXT-ANN**	**EXT-PCA-ANN**	**EXT-CCA-ANN**	**EXT-ANN-GEV**	metrics	**MAP-Lm**	**MAP-ANN**	**EXT-ANN**	**EXT-PCA-ANN**	**EXT-CCA-ANN**	**EXT-ANN-GEV**
1h							**1h**						
BIASr	*-0.009*	-0.003	-0.004	**0.001**	-0.004	0.008	**BIASr**	*-0.02*	-0.007	-0.013	**0**	-0.011	0.022
RMSE	0.044	0.043	0.043	**0.042**	**0.042**	0.049	**RMSE**	0.198	0.194	0.196	*0.191*	**0.189**	0.197
PCC	*0.103*	0.077	0.24	**0.268**	0.251	0.237	**PCC**	0.105	*0.101*	0.242	0.257	**0.272**	0.378
3h							**3h**						

BIASr	*-0.012*	**-0.009**	-0.011	**-0.009**	-0.01	0.031	**BIASr**	-0.021	**-0.019**	*-0.02*	**-0.019**	-0.02	0.060
RMSE	*0.045*	0.04	0.038	**0.037**	0.038	0.088	**RMSE**	*0.201*	0.186	**0.172**	**0.172**	**0.172**	0.276
PCC	*-0.096*	0.034	**0.405**	0.375	0.361	0.202	**PCC**	-0.082	*0.02*	**0.42**	0.387	0.389	-0.015
6h							**6h**						
BIASr	-0.007	-0.009	-0.009	*-0.011*	**-0.006**	0.030	**BIASr**	**-0.013**	-0.019	-0.02	*-0.025*	-0.014	0.057
RMSE	*0.045*	0.041	**0.038**	0.04	0.039	0.096	**RMSE**	*0.206*	**0.187**	0.171	0.178	0.175	0.279
PCC	*-0.152*	0.175	**0.395**	0.319	0.307	0.284	**PCC**	*-0.129*	0.175	**0.442**	0.375	0.369	0.082
12h							**12h**						
BIASr	-0.006	*-0.008*	-0.005	*-0.008*	**-0.004**	0.028	**BIASr**	-0.011	-0.017	**-0.01**	*-0.02*	**-0.01**	0.053
RMSE	*0.045*	0.042	**0.038**	0.041	0.04	0.098	**RMSE**	*0.205*	0.188	**0.169**	0.181	0.178	0.275
PCC	*-0.087*	0.146	**0.394**	0.242	0.255	0.235	**PCC**	*-0.092*	0.194	**0.45**	0.318	0.331	0.142
24h							**24h**						
BIASr	**-0.006**	*-0.01*	-0.007	-0.008	-0.007	0.011	**BIASr**	**-0.014**	*-0.025*	-0.018	-0.02	-0.017	0.020
RMSE	*0.044*	0.041	**0.036**	0.039	0.039	0.062	**RMSE**	*0.198*	0.185	**0.156**	0.17	0.169	0.205
PCC	*-0.07*	0.103	**0.474**	0.319	0.316	0.444	**PCC**	*-0.065*	0.134	**0.534**	0.401	0.4	0.201

Table 3: *Performance metrics for predicted 80th and 99th percentiles of dimensionless rainfall depth associated with different durations at 100 validation raingauges. For each duration, the best case among the models MAP-Lm, EXT-ANN, EXT-PCA-ANN and EXT-CCA-ANN is marked in bold for each metric, while the worst is in italic. The column EXT-ANN-GEV reports the metrics for a demonstration of the adaptability of EXT-ANN to the GEV distribution.*

It is generally possible to observe a good agreement between the metrics listed in Table 2 (scale parameter) and in Table 3 (rainfall percentiles). The EXT-ANN, EXT-PCA-ANN and EXT-CCA-ANN models show a similar performance according to all metrics. As for the scale parameter, BIASr values are discordant with the other two metrics, but always very small in all cases (a few % at most). For longer durations (i.e., 6, 12 and 24h) EXT-ANN is the best performing model according to RMSE and PCC;

488 differently, for short durations (i.e., 1 or 3h), the best performing model depends on the metric being
489 considered, but the models with preprocessing usually outperform the EXT-ANN.

490 Since the overall best performing model is in general achieved by the EXT-ANN model, we carried out a
491 detailed analysis of its behavior. Figure 5 reports the geographical distribution of the PRE of the 99^{th}
492 percentile predicted for 1 and 24h durations (panels a and b, respectively). First, no clear geographical
493 pattern of the prediction error is visible: the goodness of the prediction for both 1 and 24h does not
494 seem to be linked to elevation, nor geographical location, and shows similar geographical variability for
495 both durations. Absolute values of PRE (|PRE|) are higher than 50% in one case only for the set of 100
496 validation locations. Most of stations have low |PRE| values (i.e., |PRE|< 5% for 44 and 43 validation
497 locations for 1h and 24h duration, respectively). The number of validation locations showing
498 20%<|PRE|<50% for a duration of 1h (i.e., 9) is larger than for a 24h duration (i.e., 6).

499

500

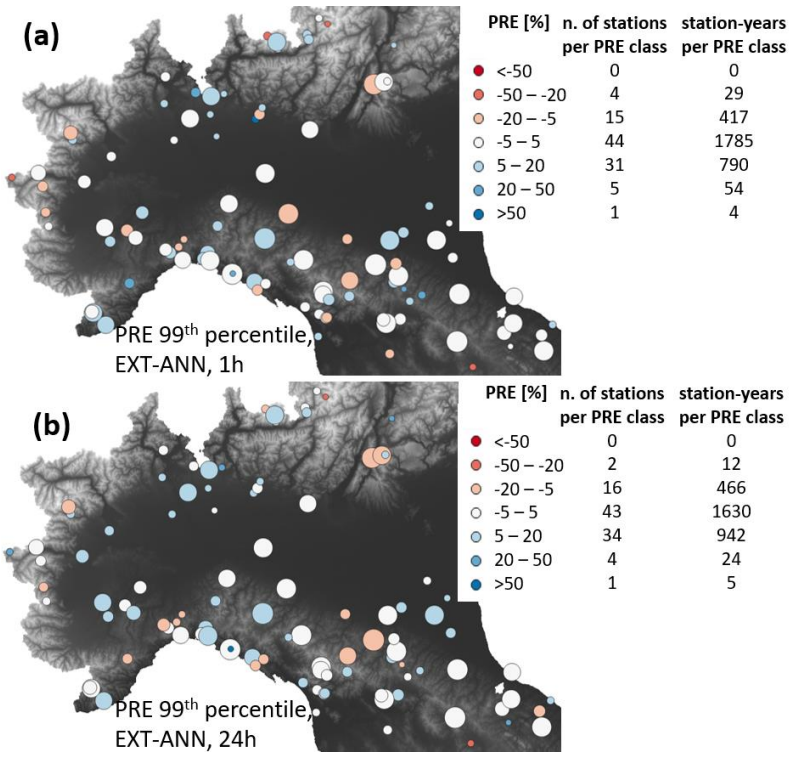

Figure 5: *Percent relative error (PRE) of EXT-ANN dimensionless 99th percentiles at 100 validation raingauges for 1h (a) and 24h (b) durations; larger circles represent longer annual maximum series. The number of test raingauges, and the corresponding station-years of data, is reported for each PRE category.*

The same analysis of PRE for the 99th percentile obtained from the MAP-Lm model is presented in Figure 6. As for the EXT-ANN model, no clear geographical pattern of the PRE is observed and most of the stations have PRE between –20% and 20% (i.e., 17+37+35 for 1h, 19+33+37 for 24h). In particular, the stations with PRE between –5% and 5% are 37 for 1h and 33 for 24h (lower numbers when compared to Figure 5), while the stations with PRE>20% or <20% are 11 for both time-intervals (i.e., 3+7+1 for 1h and 6+4+1 for 24h, higher values when compared to Figure 5).

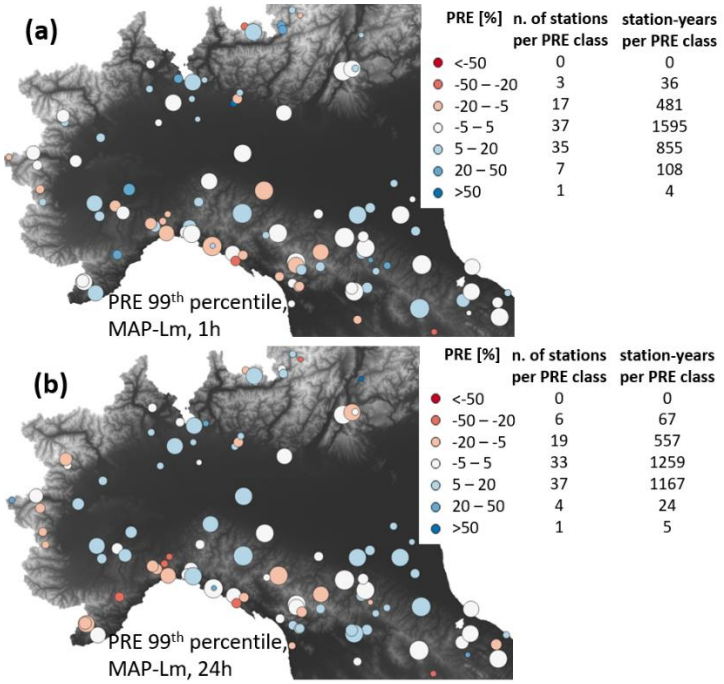

Figure 6: *Percent relative error (PRE) of MAP-Lm dimensionless 99th percentiles at 100 validation raingauges for 1h (a) and 24h (b) durations; larger circles represent longer annual maximum series. The number of test raingauges, and the corresponding station-years of data, is reported for each PRE category.*

Finally, the results of model EXT-ANN are used to obtain the location and scale parameters of a GEV distribution (see Section 4.2). Table 4 reports the global metrics obtained for the 80th and 99th percentiles of dimensionless rainfall depth (columns "EXT-ANN-GEV"). These are relative to empirical predictions of the same percentiles adopting a GEV distribution and the hybrid local/regional estimator described in Section 4.

While BIASr and RMSE are very similar to the previous case of application with the Gumbel ANN (columns "EXT-ANN" of Table 3), PCC values are significantly lower, with the exception of 1h, which has the highest PCC.

7. Interpolation across space and time-aggregation interval

One of the most innovative and useful aspects of our AI-based approach is its capability to provide predictions of the dimensionless rainfall distribution in any location (spatial interpolation) and for any time-aggregation interval (i.e., duration) between 1 and 24 hours (time-aggregation interpolation).

As an example, four stations in different geographic and climatic contexts (Table 3) are selected for time-aggregation interpolation. Figure 7 shows the Depth Duration Frequency (DDF) curves obtained with the EXT-ANN model in the four raingauges. Dimensionality was reintroduced, and consistency among percentiles ensured, by multiplying the predicted dimensionless percentiles by the mean extreme precipitation for each duration (eq. 1). The latter was obtained by applying the scale-invariance hypothesis to the mean extreme precipitation (see Burlando and Rosso, 1996) and using a power scale law between time-aggregation and mean precipitation. Since the focus of the present study is regional modelling of the growth factor of the storm index method, estimation of the index rainfall (i.e., the mean extreme rainfall depth, see Sect. 2) with multiple scaling is not discussed.

Code	Location	Record length	Mean elevation [m a.s.l.]	Minimum distance from the Adriatic coast [km]	Minimum distance from the Thyrrenic coast [km]	MAP [mm]	MASnow [mm]
9086	Codogno	64	60.28	202.49	98.18	802.58	7.28
17020	Folgaria	58	1114.7	109.60	225.73	1219.16	193.83

5143	Isola di Palanzano Centrale	70	723.13	167.62	43.18	1416.89	39.28
16126	La Verna	76	1080.65	62.29	124.64	1174.25	163.38

Table 4 – *Main characteristics of the four stations adopted for the time-aggregation interpolation application through EXT-ANN model*

Some observations can be highlighted. First, in stations 9086, 5143 and 16126, the EXT-ANN model has greater accuracy at 1h and 24h, while it is not fully capable of reproducing the fitted model at 6h and 12h; this confirms the metrics in Tables 2 and 3. Station 17020 is a case of underestimation of the EXT-ANN (see also same station in Figure 4, with PRE in -20% - -5% range), where the traditional MAP-Lm model performs better than the ANN-based one. The MAP-Lm approach has similar performances in all four stations: greater errors for longer return periods and longer durations.

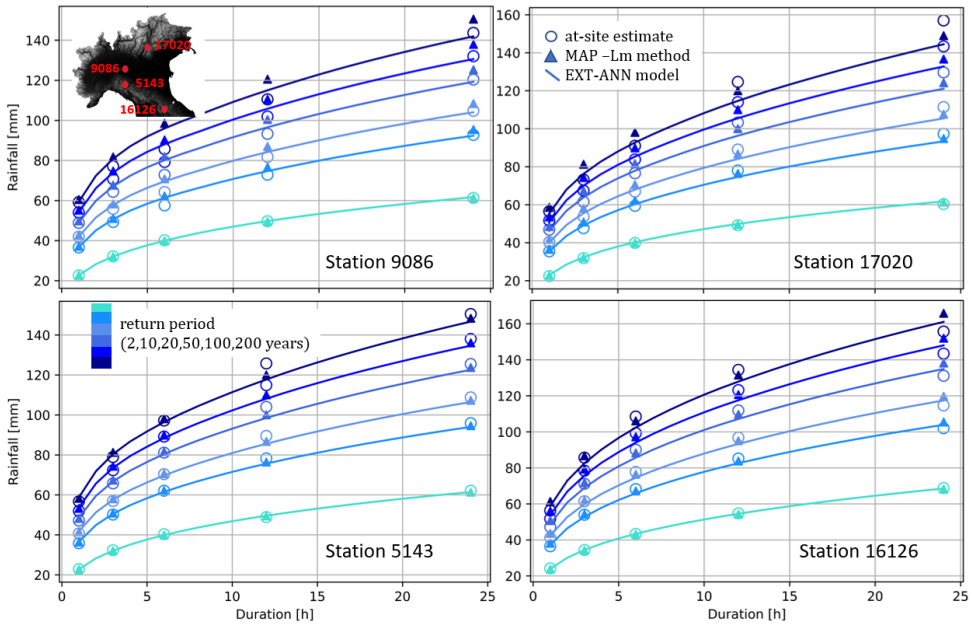

Figure 7: *DDF obtained with EXT-ANN and MAP-Lm models for stations 9086, 17020, 5143, and 16126 (see also Table 3).*

551 Regional ensemble ANN models presented here can produce a spatial interpolation of estimated
552 frequency distributions (i.e., Gumbel distribution in this study) based on the gridded discretization of the
553 study area used for retrieving the local values of the morphoclimatic indices. Panels (a) and (b) of Figure
554 8 show the scale parameters predicted by the EXT-ANN model for the dimensionless distributions of 1h
555 and 24h annual maximum rainfall depths over the drainage area of an Apennine catchment in north-
556 central Italy (i.e., Panaro river basin, drainage area ~2300 km^2). It can be observed that the average
557 value is higher for 1h duration than 24h (i.e., 0.28 against 0.25). The relation between the predicted
558 scale and the elevation is directly proportional to the MAP and is further explored in panels (c) and (d).
559 Here, a rather evident decrease of the scale parameter for 1h duration is observed when the elevation is
560 growing, while no clear regression is obtained for 24h. This seems to be in agreement with recent
561 findings of Marra et al. (2021), who observed a significant decreasing trend of the Weibull scale
562 parameters with elevation for sub-hourly durations, while no significant trend was detected for longer
563 time-intervals.

564

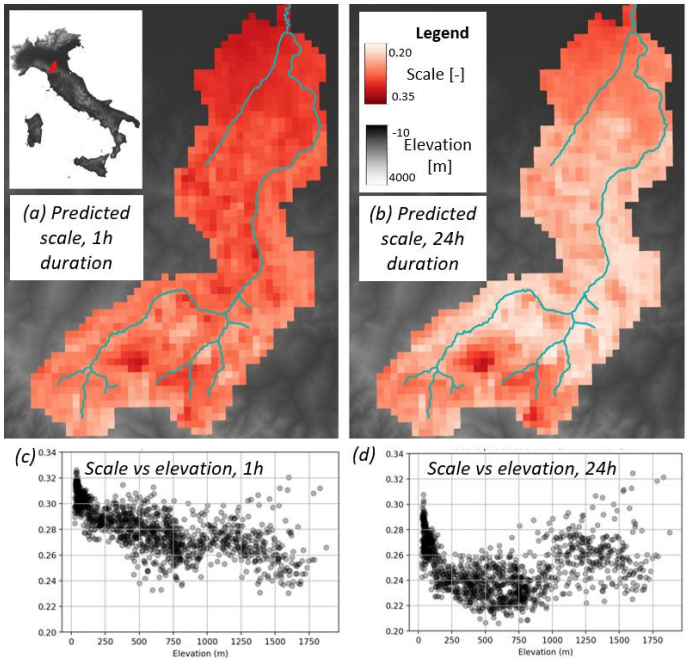

Figure 8: *Raster-based EXT-ANN prediction of Gumbel scale parameters for 1h (a) and 24h (b), obtained for an example river catchment in the study area (i.e., Panaro river catchment); the main river network is reported in light blue. Scatterplot of scale parameters against elevation values for 1h (c), and 24h (d), from raster-based prediction.*

8. Discussion

The proposed approach aims at improving the predicting ability of the traditional L-moments storm index model with the action of three combined strategies: (1) exploiting complex non-linear regional functions (i.e., through ANN ensembles), (2) increasing the amount of data used for training the regional models, and (3) increasing the number of proxies for extreme precipitation. The first two points are discussed through the comparison between MAP-Lm and MAP-ANN (subsection 8.1), while the third one regards the EXT-ANN, EXT-PCA-ANN and EXT-CCA-ANN models (subsection 8.2).

8.1 Comparing MAP-Lm with MAP-ANN

Metrics in Tables 2 and 3 show that BIASr and RMSE are very similar for MAP-Lm and EXT-ANN, while PCC has significant variations and, more in general, rather low values (i.e., lower than 0.60). This is due to the different nature of the three metrics (see Section 4): a small difference in BIASr and RMSE confirms that prediction errors from the two approaches are very similar. Anyway, the higher PCC values (with the exception of 1h time-interval) suggest that changing model type and data management strategy introduces some benefits (i.e., positive correlation between expected and predicted variables). Overall, it is evident that the MAP-ANN model has unsatisfactory accuracy (i.e., maximum PCC 0.204 for scale with 12h time-interval). However, this could be considered a good result when carefully looking at the regional relation developed within the MAP-Lm framework (see Figure 9 for 1h and 24h cases). In particular, the L-CV(MAP) relations found in the present study (see red lines in Figure 9) do not show clear and strong relationships between L-CV and MAP, especially for the 24h case. The comparison with an empirical relation reported in the literature (i.e., Di Baldassarre et al., 2006, see dotted red lines in Figure 9) suggests that when a large and morphologically and climatically complex region is considered, the classical MAP-Lm approach may not be a viable regionalization strategy. The discrepancies between the relationship identified in this study and that of Di Baldassarre et al. (2006) is more evident for long time aggregation intervals and less pronounced for short durations. In fact, 24h annual maxima are generally associated with frontal disturbances in the study region, and show a complex geographical variability of annual maxima statistics (see e.g. Mazzoglio et al., 2022). Differently, 1h annual maxima are mostly the result of convective storms, which have more spatially homogeneous statistics (see e.g. Schaefer, 1990, Alila 1999, Di Baldassarre et al. 2006).

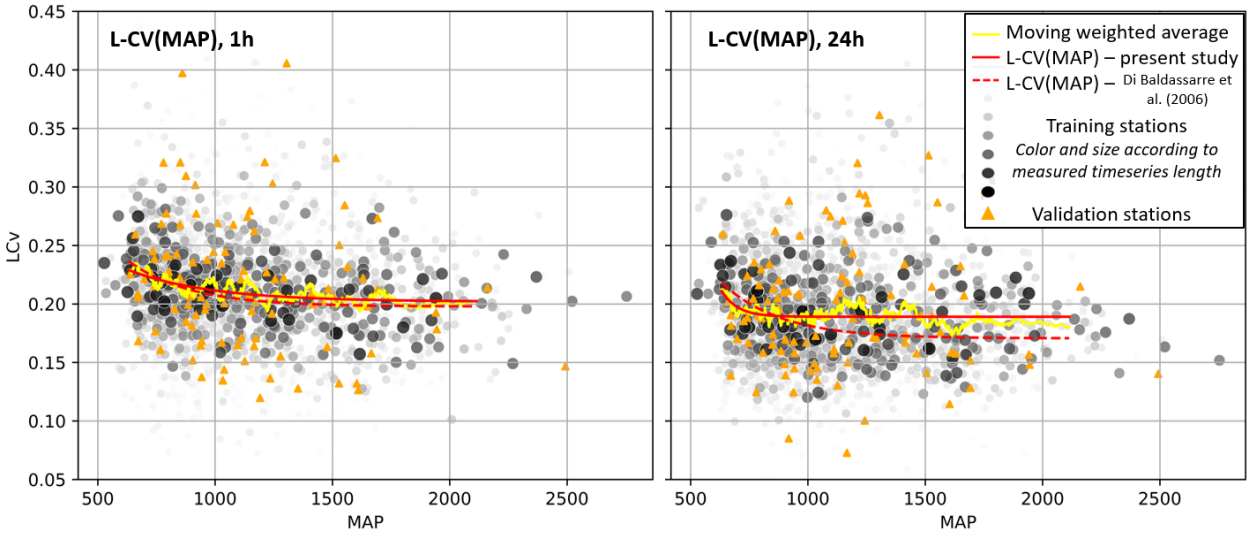

Figure 9: *Empirical L-CV and local MAP values across the study area (dots); moving weighted average (yellow line); Horton-type regional relationship L-CV(MAP) in eq. 2 fitted to the moving weighted average (red solid line) and found by Di Baldassarre et al. (2006) over north-central Italy (red dashed line).*

8.2 EXT-ANN, EXT-PCA-ANN and EXT-CCA-ANN

For any time-aggregation interval (i.e., duration), the EXT-ANN, EXT-PCA-ANN and EXT-CCA-ANN models outperform the MAP-Lm and MAP-ANN when referring to the global metrics (Tables 2 and 3). The difference is particularly significant for the PCC, which shows that the EXT- models (that make use of an EXTended set of descriptors) are much more effective in capturing the overall trend of the variables (i.e., location, scale, 80th and 99th percentiles) within the study area. However, the maximum value of PCC for the scale parameter is still very low for 1h (i.e., 0.275), and lower than 0.6 for 24h. This clearly shows that the EXT- models are more accurate when modelling rainfall phenomena with longer durations, as it is also evident from the higher number of high absolute PRE values (i.e., Percent Relative Error) for 1h (i.e., 10 cases in total out of 100) than for 24h (i.e., 7 cases) for the EXT-ANN (Figure 5). A possible reason for these results is that convection phenomena are less influenced by the morphology (see, e.g., Schaefer, 1990, and Alila, 1999), leading to lower predictive power of most of the input descriptors.

Anyway, it is worth highlighting that PRE values <-20% or >20% are mainly observed in Figure 5.a in stations where long data series are not available and the expected values (i.e., locally fitted Gumbel distributions) are less reliable, while numerous stations with longer AMS show good results (i.e., PRE values between –5% and 5%).

Also, it is interesting to note that percentiles obtained from the MAP-Lm approach are rather similar to the ones from local data frequency analysis in some cases (see Figure 7), even if the model is very simple. However, when looking at the PRE values for the dimensionless 99^{th} percentile (see Figure65), and comparing it with the one predicted with EXT-ANN, the lower accuracy of the former MAP-Lm is evident. First, gauged locations associated with high PRE values for the 99^{th} percentiles are more for MAP-Lm (i.e., 11 for 1h, and 11 for 24h, see Figure 6) than for the EXT-ANN (see above). Accordingly, locations associated with lower PRE values (i.e., 37 for 1h and 33 for 24h) are less (i.e., for EXT-ANN, 44 for 1h and 43 for 24h).

Regarding the gridded EXT-ANN predictions (Figure 8), it is difficult to objectively compare our results with previous knowledge, as studies on the link between parameters of Gumbel distributions of dimensionless annual maxima and orography are lacking. Marra et al. (2021) observed the relations between scale parameter of Weibull distributions of ordinary events and elevation in Israel. This seems to be aligned with the trends of the linear and non-linear relations found in the present study between the scale parameter and elevation for 1h and 24h (Figure 8.c and 8.d).

Since we use a large number of gauged sites that are described by several correlated indices and annual maximum series of very different length, the real signal of the regional function is expected to be disturbed by a certain noise. Thus, the actual impact of preprocessing morphological and climate descriptors is worth analyzing. Multivariate preprocessing techniques generally allow to reduce the noise, so that the models train to reproduce the signal. However, it is remarkable here that data

637 preprocessing (i.e., principal component analysis, or PCA, and canonical correlation analysis, or CCA)
638 seems to have a positive impact just for the 1h duration, while for longer durations the EXT-ANN model
639 performs the best (see Tables 2 and 3). This is a positive result, as it clearly shows how the ensemble
640 ANNs can successfully handle large datasets with several couples of variables that are strongly inter-
641 correlated (see dark colored cells in Figure 2). In general, it is not possible to understand whether or not
642 preprocessing the input data should be preferred to using the raw dataset, but some conclusions can be
643 drawn. First, preprocessing can impact the performance of the model, in a positive but also negative
644 way. Second, PCA and CCA have similar performances. Third, in absolute terms, all EXT- regional models
645 have very similar performances and prediction accuracy. Fourth, given the similar performance, it has to
646 be mentioned that reducing the dimensionality of the problem and making the models simpler through
647 preprocessing techniques has significant computational advantages in the training phase.

648 Concerning the preliminary adaptation of the proposed ANN approach to the GEV (i.e., Generalized
649 Extreme Value) distribution, the results are encouraging, as the BIASr and RMSE are very similar to the
650 ones computed for the Gumbel (Table 3). However, a correct estimation of the higher order statistical
651 moments, and therefore of shape parameters of 3- and 4-parameter distributions, remains a critical
652 aspect for the use of more flexible probability distributions. The sampling variability of the predictions of
653 GEV parameters used in this study is probably the main reason for the lower PCC values obtained for the
654 EXT-ANN-GEV relative to the EXT-ANN, which indicates a weaker linearity between ANN predictions of
655 dimensionless GEV rainfall percentiles and their empirical validation counterparts. To further investigate
656 this aspect, we computed the same performance metrics by considering only the validation stations with
657 timeseries longer than 40 years. For the sake of brevity, these results are not reported in Table 3, but an
658 improvement of the performance was observed, leading to PCC values aligned to those associated with
659 the best performing Gumbel ANN models. This confirms that the record length strongly affects the
660 training and validation of the EXT-ANN-GEV approach. Although we showcase the adaptability of the

proposed ANN approach to probability distributions with more than two parameters, dedicated studies are needed for assessing the impact and benefit of short timeseries for the models' training and validation.

In conclusion, the proposed AI-based approach shows satisfactory accuracy relative to classical regionalization methods, and significantly superior performances for time-aggregation intervals equal to or longer than 12h. It also has the advantages of being applicable over a very large study area, and allowing to model any time-aggregation interval between 1 and 24 hours, which automatizes the construction of duration-depth-frequency curves. However, some drawbacks and margins of improvements are still present. First, the accuracy with 1h is still low, which could be improved with a more complex model architecture. Second, some of the input variables (i.e., morphological and climatic descriptors) are not easy to retrieve and compute and not always available, which affects model applicability. In particular, descriptors related to the distance from the two coasts (i.e., variables 7-14, table 1) can require significant GIS-computational resources to be retrieved for a large number of points. This can be a limit specially in a raster-based or gridded application aimed to produce spatially interpolated maps as in Figure 7. Such a problem could be solved with a reliable ranking of the input descriptors' influence on the final results. However, no direct method exists for input features' ranking in ANNs, and the weights computed for the PCA and CCA are not informative, as in disagreement. Given also the case-specific meaning of this analysis, which is in contrast with the general aims of this study, this point needs to be addressed by future works.

Finally, the present work considered the 2-parameter Gumbel distribution. More flexible statistical models (e.g., 3-parameter GEV, Jenkinson, 1955; 4-parameter Kappa distribution, see e.g. Blum et al., 2017) could eventually be used. Preliminary experiments performed with a GEV distribution highlight strong potential of the approach. However, further testing of the robustness of our approach is needed

for models with more than 2 parameters in which for instance the skewness (3-parameter) and the skewness and kurtosis (4-parameter) need to be modelled.

9. Conclusions and further steps

Regional frequency analysis (RFA) is commonly adopted for estimating extreme hydrological variables such as floods or extreme rainfall where local measurements are unavailable or insufficient for at-site frequency analysis. Different approaches have been proposed for the RFA of rainfall extremes, each one characterized by specific advantages and disadvantages (see e.g. Claps et al., 2022). One of the most common drawbacks is that regional models specifically refer to a single duration or a single exceedance probability. Several approaches require the definition of a homogeneous region where the model is trained; this leads to higher accuracy. However, the applicability of the model is then limited to locations that are hydrologically similar to the homogeneous group used in the training. Moreover, most models require filtering the available gauged stations based on the length of the measured timeseries to perform reliable frequency analysis. These aspects lead to discarding a significant amount of data, which could turn out to be detrimental to the accuracy of the regional predictions in some cases.

This study proposes a new approach for estimating the growth factor within the storm index framework for extreme rainfall RFA. This is the dimensionless percentile associated with a given duration and exceedance probability. By multiplying the growth factor by the mean extreme rainfall with the same duration, the dimensional percentile can be obtained (Dalrymple, 1960). Our approach is based on ensemble unsupervised artificial neural networks (ANNs), that are capable of predicting the location and

scale parameters of a Gumbel distribution of the dimensionless rainfall for any sub-daily time aggregation interval (duration) in the 1-24h range.

The study area consists of a large region in north-central Italy, where a wide variety of morpho-climatic contexts are present. From the I^2-RED freely available dataset (Mazzoglio et al., 2020), 2338 gauged stations are selected, where measurements of annual maximum rainfall depths are available in the 1931-2019 record period for the 1, 3, 6, 12, 24h time-intervals (i.e., durations). To train the models 2238 gauged stations are used, while the remaining 100 serve as validation set.

Following one approach proposed in the literature (Di Baldassare et al., 2006) that showed good results over a significant portion of the selected study area, a baseline regional model is developed (MAP-Lm). This consists of a relationship between the L-coefficient of variation and the MAP. Then, four applications of the ANN-based approach are set up: the first (MAP-ANN) makes use of the mean annual precipitation as unique input covariate; the second (EXT-ANN) makes use of an extended number of twenty variables, including morphology (e.g., elevation, slope, aspect, distance from the coast), climate (i.e., mean and standard deviation of snow and liquid precipitation) and geographical coordinates of the stations. The fourth and fifth models (EXT-PCA-ANN and EXT-CCA-ANN, respectively) make use of the same extended dataset, but apply two different preprocessing strategies of the input morphoclimatic covariates (or descriptors), namely principal component analysis (PCA) and canonical correlation analysis (CCA).

This method is innovative for several reasons. First, it does not require the identification of a homogeneous group of sites for model training and application. Second, it uses all available annual maximum data, regardless of the length of the annual sequence (which can be very short, and even two observations). Third, training is simultaneously performed for all durations. These characteristics lead to

727 high interpolation ability, meaning that a single model can predict Gumbel distributions for the extreme
728 rainfall in every point in the spatial domain, and for any duration in the 1-24h range.

729 The performances of the regional models are analyzed through global metrics (e.g., Pearson correlation
730 coefficient, or PCC), that sum up prediction accuracy over all the validation set, and through the percent
731 relative error (PRE) at each single validation station. Results indicate that the classical approach MAP-
732 Lm appears to have low accuracy when applied to a very large and morpho-climatically heterogeneous
733 region (i.e., PCC~0.1 for 99th dimensionless percentiles of annual maximum depth for a 1h duration, and
734 PCC~-0.1 for a 24h duration). The MAP-ANN method, which uses the same input information (i.e., MAP)
735 but a different approach (i.e., simultaneous use of durations, and ANNs ensembles) shows a slightly
736 better performance, but still low accuracy. When twenty descriptors of the local morphoclimatic
737 conditions are used, ANN-based models show a significant improvement over the MAP-Lm and MAP-
738 ANN (i.e., PCC~0.3 for the 99th dimensionless percentile for 1h, and 0.5 for 24h). Even if the maximum
739 PCC are still low, when considering the local PRE over the 100 validation stations, the improvement of
740 the new approach is evident, as the number of stations with low relative error (i.e., PRE between –5%
741 and 5%) increases (i.e., 44 and 43 for EXT-ANN at 1 and 24h durations, respectively, versus 37 and 33 for
742 the MAP-Lm).

743 Also, ensemble ANNs show good ability to handle complex and heterogeneous datasets, even without
744 data preprocessing. PCA and CCA seem to have a slight positive effect in modelling short duration
745 extremes, while their impact is limited for longer durations.

746 In conclusion, based on the outcomes of our study we can affirm that using ensemble ANN models with
747 a few traditional descriptors (i.e., local MAP value as in Schaefer 1990 and similar and more recent
748 regional studies) does not lead to significant advantages over a traditional method (i.e., statistics of
749 extremes rainfall event as empirical functions of local MAP value). However, when combined with

multiple morphological and climatic descriptors, the improvement can be remarkable, particularly for annual maximum rainfall depths associated with longer time-aggregation intervals (between 12 and 24 hours in this study). Time and space interpolation ability of the ANNs over the 1-24h range and across the entire study area enable practitioners to directly obtain depth-duration-frequency curves or raster maps of rainfall extremes associated with a given duration and exceedance probability. Future analyses should build on this preliminary study and address some of the current limitations of the approach. First, methods should be further developed in order to improve the accuracy for extremes originated by convective events. Second more flexible distributions should be considered (e.g., Generalized Extreme Value). Preliminary experiments in this direction produced encouraging results. Third, some additional research should aim at identifying the most effective and descriptive morphoclimatic indices, including alternative or complementary information to the descriptors considered in this study.

Disclosure statement

The authors report there are no competing interests to declare.

Acknowledgements

This work was supported by Autorità di bacino distrettuale del fiume Po, under grant nos. L241CASTELLARIN12820, REP.128 PROT.3431. The research would not have been possible without access to the I^2-RED dataset (Mazzoglio et al., 2020), given by Paola Mazzoglio and Pierluigi Claps. The authors also gratefully acknowledge the use of free and open-source software, in particular Python (Van Rossum et al., 1995), Scikit-learn (Pedregosa et al., 2011), TensorFlow (Abadi et al., 2015), QGIS (QGIS Development Team, 2021) and GRASS GIS (GRASS Development Team, 2019).

Author contribution

Andrea Magnini: Conceptualization, Methodology, Investigation, Software, Writing – Original Draft. Michele Lombardi: Conceptualization, Coding. Taha B. M. J. Ouarda: Conceptualization, Methodology, Writing – Original Draft. Attilio Castellarin: Supervision, Conceptualization, Methodology, Writing – Original Draft.

Data availability statement

The annual maxima series used from the present study (I.e., I^2-RED) are available with restricted access on Zenodo (see Mazzoglio et al., 2020). The ISPRA BIGBANG dataset can be downloaded free of charge from: https://www.isprambiente.gov.it/pre_meteo/idro/BIGBANG_ISPRA.html. The MERIT DEM can be downloaded free of charge from: http://hydro.iis.u-tokyo.ac.jp/~yamadai/MERIT_DEM/.

References

Abadi, M., Agarwal, A., Barham, P., Brevdo, E., Chen, Z., Citro, C., Corrado, G. S., Davis, A., Dean, J., Devin, M., Ghemawat, S., Goodfellow, I., Harp, A., Irving, G., Isard, M., Jozefowicz, R., Jia, Y., Kaiser, L., Kudlur, M., Levenberg, J., Mané, D., Schuster, M., Monga, R., Moore, S., Murray, D., Olah, C., Shlens, J., Steiner, B., Sutskever, I., Talwar, K., Tucker, P., Vanhoucke, V., Vasudevan, V., Viégas, F., Vinyals, O., Warden, P., Wattenberg, M., Wicke, M., Yu, Y. and Zheng, X., 2015. TensorFlow: Large-scale machine learning on heterogeneous systems. Software available from tensorflow.org.

Alila, Y., 1999. A hierarchical approach for the regionalization of precipitation annual maxima in Canada. J. Geophys. Res. Atmospheres 104, 31645–31655. https://doi.org/10.1029/1999JD900764

Allamano, P., Claps, P., Laio, F., Thea, C., 2009. A data-based assessment of the dependence of short-duration precipitation on elevation. Physics and Chemistry of the Earth 34, 10-12, 635 – 641. Doi: 10.1016/j.pce.2009.01.001

Blöschl, G., 2011. Scaling and Regionalization in Hydrology, in: Treatise on Water Science. Elsevier, pp. 519–535. https://doi.org/10.1016/B978-0-444-53199-5.00113-5

Blum, A.G., Archfield, S.A., Vogel, R.M., 2017. The probability distribution of daily streamflow in the United States. Hydrol. Earth Syst. Sci. 21, 3093–3103. https://doi.org/10.5194/hess-21-3093-2017

Braca, G., Bussettini, M., Ducci, D., Lastoria, B., Mariani, S., 2019. Evaluation of national and regional groundwater resources under climate change scenarios using a GIS-based water budget procedure. Rendiconti Lincei Sci. Fis. E Nat. 30, 109–123. https://doi.org/10.1007/s12210-018-00757-6

Brath, A., Castellarin, A., and Montanari, A.: Assessing the reliability of regional depth-duration-frequency equations for gaged and ungaged sites, Water Resour. Res., 39(12), 1367–1379, 2003

Breiman, L., 1996a. Stacked regressions. Mach. Learn. 24, 49–64. https://doi.org/10.1007/BF00117832

Breiman, L., 1996b. Bagging predictors. Mach. Learn. 24, 123–140. https://doi.org/10.1007/BF00058655

Burlando, P., Rosso, R., 1996. Scaling and multiscaling models of depth-duration-frequency curves for storm precipitation. Journal of Hydrology, volume 187, Issues 1–2, pages 45-64. ISSN 0022-1694. https://doi.org/10.1016/S0022-1694(96)03086-7

Burn, D.H., 1990. An appraisal of the "region of influence" approach to flood frequency analysis. Hydrol. Sci. J. 35, 149–165. https://doi.org/10.1080/02626669009492415

Caldas-Alvarez, A., Augenstein, M., Ayzel, G., Barfus, K., Cherian, R., Dillenardt, L., Fauer, F., Feldmann, H., Heistermann, M., Karwat, A., Kaspar, F., Kreibich, H., Lucio-Eceiza, E. E., Meredith, E. P., Mohr, S., Niermann, D., Pfahl, S., Ruff, F., Rust, H. W., Schoppa, L., Schwitalla, T., Steidl, S., Thieken, A. H., Tradowsky, J. S., Wulfmeyer, V., and Quaas, J., 2022. Meteorological, impact and climate perspectives of the 29 June 2017 heavy precipitation event in the Berlin metropolitan area, Nat. Hazards Earth Syst. Sci., 22, 3701–3724, https://doi.org/10.5194/nhess-22-3701-2022

Camorani, G., Castellarin, A., Brath, A., 2005. Effects of land-use changes on the hydrologic response of reclamation systems, Physics and Chemistry of the Earth 30, 561-574, https://doi.org/10.1016/j.pce.2005.07.010

Castellarin, A., Merz, R., Blöschl G., 2009. Probabilistic envelope curves for extreme rainfall events. Journal of Hydrology 378 (3-4), 263-271

Castellarin, A., Burn, D.H., Brath, A., 2001. Assessing the effectiveness of hydrological similarity measures for flood frequency analysis. J. Hydrol. 241, 270–285. https://doi.org/10.1016/S0022-1694(00)00383-8

Claps, P., Ganora, D., Mazzoglio, P., 2022. Rainfall regionalization techniques, in: Rainfall. Elsevier, pp. 327–350. https://doi.org/10.1016/B978-0-12-822544-8.00013-5

Dalrymple, T., 1960. Flood frequency analysis, U.S. Geol. Surv. Water Supply Pap., 1543-A, 11–51.

Di Baldassarre, G., Castellarin, A., Brath, A., 2006. Relationships between statistics of rainfall extremes and mean annual precipitation: an application for design-storm estimation in northern central Italy. Hydrol. Earth Syst. Sci. 10, 589–601. https://doi.org/10.5194/hess-10-589-2006

Di Baldassarre, G., Laio, F., Montanari, A., 2009. Design flood estimation using model selection criteria. Phys. Chem. Earth Parts ABC 34, 606–611. https://doi.org/10.1016/j.pce.2008.10.066

Di Prinzio, M., Castellarin, A., Toth, E., 2011. Data-driven catchment classification: application to the pub problem. Hydrology and Earth System Sciences 15 (6), 1921-1935

Ghamariadyan, M., Imteaz, M.A., 2021. Prediction of Seasonal Rainfall with One-year Lead Time Using Climate Indices: A Wavelet Neural Network Scheme. Water Resour. Manag. 35, 5347–5365. https://doi.org/10.1007/s11269-021-03007-x

Grimaldi, S., Kao, S.-C., Castellarin, A., Papalexiou, S.-M., Viglione, A., Laio, F., Aksoy, H., Gedikli, A., 2011. Statistical Hydrology, in: Treatise on Water Science. Elsevier, pp. 479–517. https://doi.org/10.1016/B978-0-444-53199-5.00046-4

GRASS Development Team, 2019. Geographic Resources Analysis Support System (GRASS) Software, Version 7.6, Open Source Geospatial Foundation, https://grass.osgeo.org

Grieser, J., Staeger, T., and Schonwiese, C.-D. Estimates and uncertainties of return periods of extreme daily precipitation in Germany, Meteorol. Z., 16, 553–564, https://doi.org/10.1127/0941-2948/2007/0235

Guo, R. and Montanari, A.: Historical rainfall data in northern Italy predict larger meteorological drought hazard than climate projections, Hydrol. Earth Syst. Sci., 27, 2847–2863, https://doi.org/10.5194/hess-27-2847-2023

Hastie, T., Tibshirani, R., Friedman, J., 2009. The Elements of Statistical

Han, J., Moraga, C., 1995. The influence of the sigmoid function parameters on the speed of backpropagation learning. In: Mira, J., Sandoval, F. (eds) From Natural to Artificial Neural Computation. IWANN 1995. Lecture Notes in Computer Science, vol 930. Springer, Berlin, Heidelberg. https://doi.org/10.1007/3-540-59497-3_175

Hastie, T., Tibshirani, R., and Friedman, J., 2009. The Elements of Statistical Learning, Springer Series in Statistics, Springer New York, New York, NY, https://doi.org/10.1007/978-0-387-84858-7

Hengl, T., 2007. A Practical Guide to Geostatistical Mapping of Environmental Variables. Office for Official Publications of the European Communities, Luxembourg. ISBN 978-92-79-06904-8

Hosking, J.R.M., Wallis, J.R., 1997. Regional Frequency Analysis: An Approach Based on L-Moments, 1st ed. Cambridge University Press. https://doi.org/10.1017/CBO9780511529443

Hosking, J.R.M., Wallis, J.R., 1993. Some statistics useful in regional frequency analysis. Water Resour. Res. 29, 271–281. https://doi.org/10.1029/92WR01980

Hotelling, H., 1935. The most predictable criterion. J. Educ. Psychol. 26, 139–142. https://doi.org/10.1037/h0058165

Jain A., Nandakumar K., Ross A., 2005. Score normalization in multimodal biometric systems. Pattern Recognition, 38 (12). DOI: 10.1016/j.patcog.2005.01.012

Jenkinson, A. F., 1955. The frequency distribution of the annual maximum (or minimum) values of meteorological elements. Quarterly Journal of the Royal Meteorological Society. 81 (348): 158–171. doi:10.1002/qj.49708134804

Jolliffe, I.T., 2002. Principal component analysis, 2nd ed. ed, Springer series in statistics. Springer, New York.

Kidd, C., Becker, A., Huffman, G.J., Muller, C.L., Joe, P., Skofronick-Jackson, G., Kirschbaum, D.B., 2017. So, How Much of the Earth's Surface Is Covered by Rain Gauges? Bull. Am. Meteorol. Soc. 98, 69–78. https://doi.org/10.1175/BAMS-D-14-00283.1

Koutsoyiannis, D., 2007. A Critical Review of Probability of Extreme Rainfall: Principles and Models, in: Vassilopoulos, A., Ashley, R., Zevenbergen, C., Pasche, E., Garvin, S. (Eds.), Advances in Urban Flood Management. Taylor & Francis, pp. 139–166. https://doi.org/10.1201/9780203945988.ch7

Koutsoyiannis, D., 2004. Statistics of extremes and estimation of extreme rainfall: I. Theoretical investigation / Statistiques de valeurs extrêmes et estimation de précipitations extrêmes: I. Recherche théorique, Hydrological Sciences Journal, 49:4, 590, DOI: 10.1623/hysj.49.4.575.54430

Koutsoyiannis, D., Baloutsos, G., 2000. Analysis of a Long Record of Annual Maximum Rainfall in Athens, Greece, and Design Rainfall Inferences. Natural Hazards 22, 29–48. https://doi.org/10.1023/A:1008001312219

Koutsoyiannis D., Kozonis D., Manetas A., 1998. A mathematical framework for studying rainfall intensity-duration-frequency relationships. Journal of Hydrology, 206 (1-2), pp. 118 - 135. DOI: 10.1016/S0022-1694(98)00097-3

Krige, D. G., 1951. A statistical approach to some mine valuations and allied problems at the Witwatersrand, Master's thesis of the University of Witwatersrand

Libertino, A., Allamano, P., Laio, F., Claps, P., 2018. Regional-scale analysis of extreme precipitation from short and fragmented records. Adv. Water Resour. 112, 147–159. https://doi.org/10.1016/j.advwatres.2017.12.015

Marra, F., Armon, M., Borga, M., and Morin, E., 2021. Orographic effect on extreme precipitation statistics peaks at hourly time scales, Geophys. Res. Lett., 48, e2020GL091498, https://doi.org/10.1029/2020GL091498

Matheron, G., 1963. Principles of geostatistics. Economic Geology, 58:1246–1266

Mazzoglio, P., Butera, I., Alvioli, M., and Claps, P., 2022. The role of morphology in the spatial distribution of short-duration rainfall extremes in Italy, Hydrol. Earth Syst. Sci., 26, 1659–1672, https://doi.org/10.5194/hess-26-1659-2022.

Mazzoglio, P., Butera, I., Claps, P., 2020. I2-RED: A Massive Update and Quality Control of the Italian Annual Extreme Rainfall Dataset. Water 12, 3308. https://doi.org/10.3390/w12123308

Milligan, G.W., Cooper, M.C. A study of standardization of variables in cluster analysis. Journal of Classification 5, 181–204 (1988). https://doi.org/10.1007/BF01897163

Modarres, R., Sarhadi, A., 2011. Statistically-based regionalization of rainfall climates of Iran. Glob. Planet. Change 75, 67–75. https://doi.org/10.1016/j.gloplacha.2010.10.009

Maity, R., 2018. Statistical methods in hydrology and hydroclimatology, Springer Nature Singapore Pte Ltd., Singapore, https://doi.org/10.1007/978-981-10-8779-0

Msilini, A., Masselot, P., Ouarda, T.B.M.J., 2020. Regional Frequency Analysis at Ungauged Sites with Multivariate Adaptive Regression Splines. J. Hydrometeorol. 21, 2777–2792. https://doi.org/10.1175/JHM-D-19-0213.1

Msilini, A., Ouarda, T.B.M.J., Masselot, P., 2022. Evaluation of additional physiographical variables characterising drainage network systems in regional frequency analysis, a Quebec watersheds case-study. Stoch. Environ. Res. Risk Assess. 36, 331–351. https://doi.org/10.1007/s00477-021-02109-7

Ngongondo, C.S., Xu, C.-Y., Tallaksen, L.M., Alemaw, B., Chirwa, T., 2011. Regional frequency analysis of rainfall extremes in Southern Malawi using the index rainfall and L-moments approaches. Stoch. Environ. Res. Risk Assess. 25, 939–955. https://doi.org/10.1007/s00477-011-0480-x

Ouali, D., Chebana, F., Ouarda, T.B.M.J., 2016a. Quantile Regression in Regional Frequency Analysis: A Better Exploitation of the Available Information. J. Hydrometeorol. 17, 1869–1883. https://doi.org/10.1175/JHM-D-15-0187.1

Ouali, D., Chebana, F., Ouarda, T.B.M.J., 2016b. Non-linear canonical correlation analysis in regional frequency analysis. Stoch. Environ. Res. Risk Assess. 30, 449–462. https://doi.org/10.1007/s00477-015-1092-7

Ouarda, T.B.M.J., Girard, C., Cavadias, G. and B. Bobée, 2001. Regional flood frequency estimation with canonical correlation analysis. Journal of Hydrology. 254(1-4): 157-173

Ouarda, T.B.M.J., Shu, C., 2009. Regional low-flow frequency analysis using single and ensemble artificial neural networks: REGIONAL LOW-FLOW ANALYSIS. Water Resour. Res. 45. https://doi.org/10.1029/2008WR007196

Ouarda, T.B.M.J., Yousef, L.A., Charron, C., 2019. Non-stationary intensity-duration-frequency curves integrating information concerning teleconnections and climate change. Int. J. Climatol. 2019; 39: 2306–2323. https://doi.org/10.1002/joc.5953

Papalexiou, S. M., AghaKouchak, A., & Foufoula-Georgiou, E., 2018. A diagnostic framework for understanding climatology of tails of hourly precipitation extremes in the United States. Water Resources Research, 54, 6725–6738. https://doi.org/10.1029/2018WR022732

Papalexiou, S. M., and Koutsoyiannis, D., 2013. Battle of extreme value distributions: A global survey on extreme daily rainfall, Water Resour. Res., 49, doi:10.1029/2012WR012557

Pedregosa, F., Varoquaux, G., Gramfort, A., Michel, V., Thirion, B., Grisel, O., Blondel, M., Müller, A., Nothman, J., Louppe, G., Prettenhofer, P., Weiss, R., Dubourg, V., Vanderplas, J., Passos, A., Cournapeau, D., Brucher, M., Perrot, M., and Duchesnay, É., 2011. Scikit-learn: Machine Learning in Python, arXiv [preprint], J. Mach. Learn. Res., 12, arxiv:1201.0490.

Persiano, S., Ferri, E., Antolini, G., Domeneghetti, A., Pavan, V., Castellarin, 2020, A. Changes in seasonality and magnitude of sub-daily rainfall extremes in Emilia-Romagna (Italy) and potential influence on regional rainfall frequency estimation. Journal of Hydrology: Regional Studies 32, 100751

Piper, D., Kunz, M., Ehmele, F., Mohr, S., Mühr, B., Kron, A., and Daniell, J., 2016. Exceptional sequence of severe thunderstorms and related flash floods in May and June 2016 in Germany. Part I:

941 Meteorological background, Nat. Hazards Earth Syst. Sci., 16, 2835–2850,
942 https://doi.org/10.5194/nhess-16-2835-2016

943 Requena, A.I., Ouarda, T.B.M.J. and Chebana, F., 2017. Flood frequency analysis at ungauged sites based
944 on regionally estimated streamflows, Journal of Hydrometeorology, 18(9): 2521-2539. doi:10.1175/jhm-
945 d-16-0143.1

946 Requena, A.I., Chebana, F. and Ouarda, T.B.M.J., 2018. A functional framework for flow-duration-curve
947 and daily streamflow estimation at ungauged sites, Advances in Water Resources, 113: 328-340.
948 doi:10.1016/j.advwatres.2018.01.019

949 Schaefer, M.G., 1990. Regional analyses of precipitation annual maxima in Washington State. Water
950 Resour. Res. 26, 119–131. https://doi.org/10.1029/WR026i001p00119

951 Shehu, B., Willems, W., Stockel, H., Thiele, L.-B., and Haberlandt, U., 2023. Regionalisation of rainfall
952 depth–duration–frequency curves with different data types in Germany, Hydrol. Earth Syst. Sci., 27,
953 1109–1132, https://doi.org/10.5194/hess-27-1109-2023.

954 Shu, C., Burn, D.H., 2004. Artificial neural network ensembles and their application in pooled flood
955 frequency analysis: ARTIFICIAL NEURAL NETWORK ENSEMBLES. Water Resour. Res. 40.
956 https://doi.org/10.1029/2003WR002816

957 Shu, C., Ouarda, T.B.M.J., 2007. Flood frequency analysis at ungauged sites using artificial neural
958 networks in canonical correlation analysis physiographic space. Water Resour. Res. 43.
959 https://doi.org/10.1029/2006WR005142

960 Skøien, J.O., Merz, R., Blöschl, G., 2006. Top-kriging - geostatistics on stream networks. Hydrol. Earth
961 Syst. Sci. 10, 277–287. https://doi.org/10.5194/hess-10-277-2006

962 Soltani, S., Helfi, R., Almasi, P., Modarres, R., 2017. Regionalization of Rainfall Intensity-Duration-
963 Frequency using a Simple Scaling Model. Water Resour. Manag. 31, 4253–4273.
964 https://doi.org/10.1007/s11269-017-1744-0

965 Svensson, C., Jones, D.A., 2010. Review of rainfall frequency estimation methods: Review of rainfall
966 frequency estimation methods. J. Flood Risk Manag. 3, 296–313. https://doi.org/10.1111/j.1753-
967 318X.2010.01079.x

968 Van den Besselaar, E. J. M., Klein Tank, A. M. G., and Buishand, T. A., 2013. Trends in European
969 precipitation extremes over 1951–2010, Int. J. Climatol., 33, 2682–2689,
970 https://doi.org/10.1002/joc.3619

971 Van Rossum, G. and Drake Jr, F. L., 1995. Python reference manual, Centrum voor Wiskunde en
972 Informatica Amsterdam, https://ir.cwi. nl/pub/5008 (last access: 13 June 2023)

973 Velázquez, J.A., Anctil, F., Ramos, M.H., Perrin, C., 2011. Can a multi-model approach improve
974 hydrological ensemble forecasting? A study on 29 French catchments using 16 hydrological model
975 structures. Adv. Geosci. 29, 33–42. https://doi.org/10.5194/adgeo-29-33-2011

976 Xu, Y., Goodacre, R. On Splitting Training and Validation Set: A Comparative Study of Cross-Validation,
977 Bootstrap and Systematic Sampling for Estimating the Generalization Performance of Supervised
978 Learning. J. Anal. Test. 2, 249–262 (2018)

979 Yamazaki, D., Ikeshima, D., Tawatari, R., Yamaguchi, T., O'Loughlin, F., Neal, J.C., Sampson, C.C., Kanae,
980 S., Bates, P.D., 2017. A high-accuracy map of global terrain elevations: Accurate Global Terrain Elevation
981 map. Geophys. Res. Lett. 44, 5844–5853. https://doi.org/10.1002/2017GL072874

982